The isotropic–nematic phase transition in uniaxial hard ellipsoid fluids: Coexistence data and the approach to the Onsager limit

Philip J. Camp, Carl P. Mason, and Michael P. Allen
H. H. Wills Physics Laboratory, Royal Fort, Tyndall Avenue, Bristol, BS8 1TL, United Kingdom

Anjali A. Khare and David A. Kofke
Department of Chemical Engineering, State University of New York at Buffalo, Buffalo, New York 14260-4200

(Received 15 April 1996; accepted 7 May 1996)

The isotropic–nematic (I-N) phase transition in hard ellipsoid fluids has been studied by computer simulation, using the Gibbs–Duhem integration technique introduced by Kofke; and theoretically, using Onsager theory and the Parsons–Lee improvement. In the simulations, the I-N coexistence line is mapped out in the P–x plane, where P is the pressure and x is the elongation, by numerically integrating a Clapeyron-like first-order differential equation, using constant-pressure simulation data for the two coexisting phases. The elongation range $5 \leqslant x \leqslant 20$ has been studied, using independent starting points provided by chemical potential calculations and thermodynamic integration of the equation of state at $x = 5,20$, plus a direct Gibbs ensemble simulation at $x = 20$. The Onsager–Parsons–Lee theory has been applied to the I-N phase transition for aspect ratios up to $x = 1000$, affording an accurate investigation of the approach to the Onsager limit for this model. This involved the numerical computation of the orientation-dependent second virial coefficient in a way that avoids expansions in Legendre polynomials, so as to be accurate at high elongation. Over the elongation range studied here, agreement between simulation and the Parsons–Lee theory is good.
 [S0021-9606(96)50231-X]

I. INTRODUCTION

Computer simulation of simple model fluids has a long history, and has provided considerable insight into the stability of phases and the transitions between them.[1,2] Unfortunately direct computer simulations of coexisting phases are prone to finite-size effects: the interfacial contribution to the free energy is significant because of the surface-to-volume ratio. Consequently a great deal of effort has been spent on devising simulation techniques that eliminate the simulation of an interface.

The location of first-order phase transitions implies determining state points for which temperature T, pressure P, and chemical potential μ are equal in the two phases; calculating μ in a simulation can be problematic. Direct test-particle insertion in both phases[3] becomes inefficient for dense fluids, and for fluids of highly nonspherical molecules. Of many suggested improvements, methods based on gradual insertion or growth of the test particle[4,5] seem to be reliable and generally applicable, if unavoidably expensive in computer time. Given reference values of $TP\mu$ in each phase, thermodynamic integration then allows location of the state points where they become equal, and this will be most efficient and accurate if the reference points are quite close to the transition. *Automatic* location of the coexistence points is facilitated by the Gibbs simulation technique, introduced by Panagiotopoulos.[6,7] This method simultaneously simulates two bulk phases which exchange volume and particles in a way that guarantees equality of pressures and chemical potentials. Like test-particle insertion, the efficiency of the method is limited by the ease of particle transfer between the two boxes, and this worsens as fluid density, and molecular non-sphericity, increase.

Once a coexistence point has been determined, the Gibbs–Duhem integration method introduced by Kofke[8,9] allows one to trace out a coexistence curve as temperature, or some other parameter, is varied. The method involves the formulation of a Clapeyron-like equation: a first-order differential equation giving the derivative of (say) the coexistence pressure with respect to an independent thermodynamic variable. This governing differential equation is then solved numerically with a predictor–corrector algorithm and constant-pressure simulation data for the coexisting phases. The starting datum for the integration has to be determined by some other means, as discussed above. Kofke illustrated the method through application to liquid–vapor coexistence in a Lennard-Jones 12,6-fluid.[8,9] Subsequent work has applied the Gibbs–Duhem technique to a range of phase equilibria: the triple point in Lennard-Jones binary mixtures, where the composition was the independent variable;[10] the triple point in a fluid interacting via a Lennard-Jones (m,n)-potential, varying m and n to construct a mutation pathway from a (12,6)-fluid to a square-well fluid;[10] the fluid–solid coexistence line in soft spheres interacting *via* a $1/r^n$ potential, varying $s = 1/n$ ($s = 0$ corresponds to hard spheres);[11,12] the fluid–solid coexistence and sublimation lines in Lennard-Jones (12,6)-fluids, varying T;[13] the isotropic–nematic transition in semiflexible polymers, where the persistence length was the independent variable.[14]

In the present work we study the isotropic–nematic (I-N) liquid crystal phase transition in fluids composed of hard prolate ellipsoids of revolution. A uniaxial ellipsoid of revo-

lution is characterized by its elongation, x, the ratio of the major and minor semiaxes, a and b respectively. For this kind of model the temperature T plays a trivial role in the thermodynamics, and we formally set $k_BT=1$ throughout, where k_B is Boltzmann's constant; our interest lies in the transition pressure and coexisting densities for each elongation. Free energy calculations, along with thermodynamic integration, have been used to locate the I-N transition for hard ellipsoid fluids with $x=3,2.75,1/2.75,1/3$.[15] For more extreme elongations, the nematic order parameter variation with density has been used to locate the transition approximately[16–18] but no free energy calculations have been performed. To do so, for each elongation separately, would be expensive, especially since for $3\leqslant x\leqslant 10$, the I-N transition density is too high for either efficient direct test-particle insertion, or the Gibbs ensemble. In the current work, we use a particle growth technique to determine the coexistence points for $x=5$, and direct test-particle insertion plus Gibbs ensemble simulation for $x=20$. Then we integrate along the I-N coexistence line $x=5\rightarrow 10$ and $x=20\rightarrow 10$, providing coexistence data at several points in between, and check the accuracy of the method by approaching $x=10$ along two completely independent routes.

Theoretical studies of the I-N transition in hard ellipsoid fluids have revolved around Onsager's theory,[19] which is a simple form of density functional theory. The free energy is expressed as a contribution from the entropy of mixing of differently oriented particles (treated as different species) plus a virial expansion in the density, $\rho=N/V$. The virial coefficients, B_n, arise from excluded volume interactions which are orientation dependent. Both the entropy and excluded-volume terms are functionals of the orientational distribution function (ODF) $f(\mathbf{e})$ where $\mathbf{e}\equiv\varphi\theta$ is a unit vector, or equivalently a pair of polar angles, defining the molecular orientation. The free energy is minimized with respect to $f(\mathbf{e})$, and all of the thermodynamic quantities and phase behavior follow. Competition between the orientational entropy and the excluded volume interactions gives rise to the I-N phase transition. In the original Onsager theory, the virial expansion is truncated at the B_2 term, and the method owes its success to the rapid convergence $\overline{B_n}/\overline{B_2}^{n-1}\rightarrow 0$ at asymptotically large elongations.[19] At intermediate elongations, however, the virial expansion is slow to converge and so the higher virial coefficients must be taken into account. This can be done directly,[20,21] by resummation theories such as the Barboy and Gelbart y-expansion,[20–24] or by renormalized two-particle theories such as that due to Parsons[25] and Lee.[26,27] In this paper we deal with this last formulation.

The input for the Onsager and Parsons–Lee theories is $\overline{B_2}$ expressed as an integral involving $f(\mathbf{e})$ and the orientation-dependent second virial coefficient $B_2(\mathbf{e}\cdot\mathbf{e}')$. In the past, the latter has been represented as an expansion in Legendre polynomials.[21,26] This expansion converges more slowly as x is increased. Consequently, when studying ellipsoids of high elongation, many expansion coefficients are needed to accurately represent $B_2(\mathbf{e}\cdot\mathbf{e}')$, and the high-order expansion coefficients become difficult to determine accurately. The truncation error for a given number of terms in the expansion may be gauged by calculating B_2 in a system of aligned ellipsoids.[21] In the present work we avoid these problems by evaluating $B_2(\mathbf{e}\cdot\mathbf{e}')$ essentially exactly; this enables us to investigate the predictions of the Onsager and Parsons–Lee theories for large elongations.

This paper is organized as follows. Section II covers the Onsager theory and its refinement by Parsons and Lee; in Sec. II C we present the method used to compute orientation-dependent second virial coefficients. Section III sets out the simulation techniques used in this study, especially the formulation of the governing differential equation for the Gibbs–Duhem integration technique, and the scheme adopted for solving this equation, in Sec. III B. In Sec. IV we describe the computational details of the simulations we have conducted both to determine coexistence points at specific values of elongation and to carry through Gibbs–Duhem integration along the coexistence line. The results are presented in Sec. V, and Sec. VI concludes the paper.

II. THEORY

The Helmholtz free energy F of N hard elongated particles in a volume V, with number density $\rho=N/V$, considered as a mixture of species having different orientations, is

$$\frac{\beta F}{N}=\ln\rho\Lambda^3-1+\int d\mathbf{e}\, f(\mathbf{e})\ln 4\pi f(\mathbf{e})+\sum_{n=2}^{\infty}\frac{\overline{B_n}}{n-1}\rho^{n-1}. \tag{1}$$

Here $\beta=1/k_BT$. The first term on the right is the ideal contribution to the free energy; Λ is the de Broglie thermal wavelength. The second term is the contribution from the orientational entropy of mixing, which depends on $f(\mathbf{e})$, the orientational distribution function (ODF), where $\mathbf{e}$ is the principal molecular axis unit vector. $f(\mathbf{e})$ satisfies the normalization condition

$$\int d\mathbf{e}\, f(\mathbf{e})=1, \tag{2}$$

thus in the isotropic phase $f(\mathbf{e})=1/4\pi$ and the orientational entropy is zero. The terms in $B_n\rho^{n-1}$ represent the excluded volume interactions between n particles. For example, $B_2\rho$ represents pairwise interactions, and B_2 is itself a functional of the ODF

$$\overline{B_2}=\int d\mathbf{e}\, d\mathbf{e}' f(\mathbf{e})f(\mathbf{e}')B_2(\mathbf{e}\cdot\mathbf{e}'). \tag{3}$$

$B_2(\mathbf{e}\cdot\mathbf{e}')$ is the orientation-dependent second virial coefficient and is equal to half the excluded volume of two nonspherical hard bodies with orientation vectors $\mathbf{e}$ and $\mathbf{e}'$. Evaluating this quantity is the subject of Sec. II C.

A. Onsager theory

The Onsager theory of orientational ordering in hard elongated particles[19] involves minimising the free energy functional F, truncated at B_2, with respect to variations of the ODF. The relevant expressions are

$$\frac{\beta F}{N}=\ln\,\rho\Lambda^3-1+\int d\mathbf{e}\; f(\mathbf{e})\ln\,4\pi f(\mathbf{e})+\overline{B_2}\rho, \tag{4a}$$

$$\beta P/\rho=1+\overline{B_2}\rho, \tag{4b}$$

$$\beta\mu=\ln\,\rho\Lambda^3+\int d\mathbf{e}\; f(\mathbf{e})\ln\,4\pi f(\mathbf{e})+2\overline{B_2}\rho\,, \tag{4c}$$

$$f(\mathbf{e})=C_1\,\exp\left\{-2\rho\int d\mathbf{e}'\; f(\mathbf{e}')B_2(\mathbf{e}\cdot\mathbf{e}')\right\}. \tag{4d}$$

Equation (4d) results from functional differentiation of Eq. (4a) subject to the normalization condition; C_1 is the normalization constant. This is a self-consistent equation for $f(\mathbf{e})$, which is solved numerically, given a form for $B_2(\mathbf{e}\cdot\mathbf{e}')$. Below the critical density there is only one solution, which corresponds to the isotropic phase, i.e. $f(\mathbf{e})=1/4\pi$. Above the transition density, a nematic solution also exists. The order parameter, S, is given by

$$S=\left\langle \tfrac{3}{2}\cos^2\theta-\tfrac{1}{2}\right\rangle=\int d\mathbf{e}\; f(\mathbf{e})\left(\tfrac{3}{2}\cos^2\theta-\tfrac{1}{2}\right), \tag{5}$$

where θ is the polar angle between the director and a particle orientation vector. At phase coexistence the pressures and chemical potentials in the two phases are equal, giving two simultaneous equations to be solved for $\rho_{\rm iso}$ and $\rho_{\rm nem}$, the isotropic and nematic coexistence densities, respectively.

B. Parsons–Lee theory

Improving the original theory, by direct inclusion of higher virial coefficients, is possible but complicated.[20,21] The theory may be improved in a more tractable way by resumming higher virial coefficients in a y-expansion.[20–24] An alternative approach, which we adopt here, is due to Parsons[25] and Lee.[26,27] The Carnahan–Starling expression for the free-energy of hard spheres is applied to the system of interest, using the (orientationally averaged) second virial coefficient of the ellipsoids as a scaling factor. This approach has been shown to be surprisingly successful at predicting the I-N transition parameters, for $x=3$.[17] Like the y-expansion, it clearly incorporates some many-body effects in an average way, while requiring only explicit knowledge of two-body excluded volumes, which makes it extremely easy to use. The relevant expressions are

$$\frac{\beta F}{N}=\ln\,\rho\Lambda^3-1+\int d\mathbf{e}\; f(\mathbf{e})\ln\,4\pi f(\mathbf{e})+(\overline{B_2}/4v_0)\frac{\phi(4-3\phi)}{(1-\phi)^2}\,, \tag{6a}$$

$$\frac{\beta P}{\rho}=\frac{(1+[(\overline{B_2}/v_0)-3]\phi+[3-(\overline{B_2}/2v_0)]\phi^2-\phi^3)}{(1-\phi)^3}\,, \tag{6b}$$

$$\beta\mu=\ln\,\rho\Lambda^3+\int d\mathbf{e}\; f(\mathbf{e})\ln\,4\pi f(\mathbf{e})+(\overline{B_2}/4v_0)\frac{8\phi-9\phi^2+3\phi^3}{(1-\phi)^3}\,, \tag{6c}$$

$$f(\mathbf{e})=C_1\,\exp\left\{-\frac{2\phi(4-3\phi)}{(1-\phi)^2}\int d\mathbf{e}'\; f(\mathbf{e}')\frac{B_2(\mathbf{e}\cdot\mathbf{e}')}{4v_0}\right\}. \tag{6d}$$

In the above, $\phi=\rho v_0$ is the packing fraction. For hard spheres, the orientational variables disappear, $B_2(\mathbf{e}\cdot\mathbf{e}')=\overline{B_2}=4v_0$, and the usual Carnahan–Starling equations[28] are recovered.

The method of solution of the above equations is exactly the same as described in the previous section. Both the original Onsager theory and the Parsons–Lee modification rely on accurate calculation of the pair-excluded volume $B_2(\mathbf{e}\cdot\mathbf{e}')$. We turn to this now.

C. Calculation of $B_2(\mathbf{e}\cdot\mathbf{e}')$

For hard potentials the second virial coefficient $B_2(\mathbf{e}\cdot\mathbf{e}')$ is simply half of the excluded volume of the oriented particles. Previous attempts to describe the dependence of the overlap volume on the relative orientation have employed expansions in an orthogonal rotational basis.[21,29,30] For our case, this takes the form

$$B_2(\mathbf{e}\cdot\mathbf{e}')=B_{2,0}+\sum_{n=1}^{\infty}B_{2,n}P_n(\mathbf{e}\cdot\mathbf{e}'), \tag{7}$$

where the expansion coefficients $B_{2,n}$ are given in Ref. 21 and P_n is the nth Legendre polynomial. For axiosymmetric ($D_{\infty h}$) particles this expansion can be simplified since only even-n terms need to be included.

This approach is particularly convenient if it is applied in an Onsager-type treatment that has the ODF expressed in terms of the same basis set. However, the accuracy of the approach deteriorates as one considers ellipsoids of increasingly long aspect ratio. Comparison of $\overline{B_2}$ for perfectly aligned ellipsoids[21] gives an idea of the magnitude of this error. $\overline{B}_2^{\parallel}=B_2^{\parallel}\equiv B_2(\mathbf{e}\cdot\mathbf{e}'=1)$ should equal the hard sphere second virial coefficient, i.e., $B_2^{\parallel}/4v_0=1$. In Table I we present $B_2^{\parallel}/4v_0$ for ellipsoids of elongation $x=5$ to $x=20$ as calculated with terms up to 10th order in the Legendre polynomial expansion. As expected, the ratio rises from unity as the elongation is increased: the truncation error is less than 4% for $1\leqslant x\leqslant 10$, but rises to 21% for $x=20$. Thus, we expect the predictions of Onsager and Parsons theories to be subject to error at higher elongations, unless a different approach is used.

To study the approach to the Onsager limit it is necessary to have a means for computing the overlap volume of two oriented convex bodies of arbitrarily large aspect ratio. Expressions of this sort are available for very few models: circular cylinders, spherocylinders,[19] and (more generally) spheroplatelets.[31,32] The result for spheroplatelets is particularly useful in that it may be applied to biaxial and nonidentical particles. We present in this section an analogous algorithm for computing the overlap volume of two arbitrary ellipsoids. Although our interest in the present study is with identical, uniaxial ellipsoids, the method described in this

TABLE I. Properties predicted by the Parsons theory (P) and the Onsager theory (O) for the isotropic–nematic phase transition in hard uniaxial ellipsoid fluids. ''a'' refers to the exact expression for $B_2(\mathbf{e}\cdot\mathbf{e}')$ for which $B_2^{\parallel}/4v_0=1$, ''b'' refers to the expansion.

	βP		$\rho_{\rm iso}/\rho_{\rm cp}$		$\rho_{\rm nem}/\rho_{\rm cp}$		S		
x	P	O	P	O	P	O	P	O	$B_2^{\parallel}/4v_0$
5.0 a	8.3904	9.2490	0.5242	0.9957	0.5472	1.0703	0.6133	0.6029	
b	8.3977		0.5244		0.5478		0.6181		1.0011
6.0 a	6.0090	6.5707	0.4554	0.7770	0.4828	0.8484	0.6424	0.6307	
b	6.0168		0.4556		0.4836		0.6485		1.0040
7.0 a	4.6632	5.0652	0.4029	0.6378	0.4335	0.7075	0.6652	0.6526	
b	4.6712		0.4033		0.4346		0.6723		1.0090
8.0 a	3.8078	4.1122	0.3617	0.5413	0.3944	0.6082	0.6834	0.6702	
b	3.8137		0.3619		0.3956		0.6910		1.0157
9.0 a	3.2184	3.4586	0.3283	0.4706	0.3624	0.5346	0.6978	0.6845	
b	3.2238		0.3286		0.3637		0.7064		1.0244
10.0 a	2.7889	2.9837	0.3007	0.4164	0.3355	0.4776	0.7096	0.6963	
b	2.7931		0.3009		0.3369		0.7188		1.0348
12.5 a	2.0963	2.2226	0.2489	0.3238	0.2840	0.3786	0.7310	0.7180	
15.0 a	1.6838	1.7728	0.2126	0.2652	0.2467	0.3146	0.7451	0.7326	
b	1.6851		0.2127		0.2482		0.7563		1.1090
20.0 a	1.2137	1.2651	0.1649	0.1951	0.1959	0.2359	0.7618	0.7507	
b	1.2139		0.1650		0.1976		0.7743		1.2104
30.0 a	0.7841	0.8078	0.1142	0.1280	0.1391	0.1578	0.7765	0.7678	
50.0 a	0.4622	0.4711	0.0709	0.0760	0.0881	0.0952	0.7859	0.7800	
100.0 a	0.2292	0.2315	0.0365	0.0378	0.0460	0.0478	0.7907	0.7873	
200.0 a	0.1144	0.1150	0.0185	0.0189	0.0235	0.0240	0.7921	0.7904	
300.0 a	0.0763	0.0765	0.0124	0.0126	0.0158	0.0160	0.7923	0.7912	
500.0 a	0.0458	0.0458	0.0075	0.0075	0.0095	0.0096	0.7925	0.7918	
700.0 a	0.0327	0.0327	0.0054	0.0054	0.0068	0.0069	0.7925	0.7920	
1000.0 a	0.0229	0.0229	0.0038	0.0038	0.0048	0.0048	0.7925	0.7922	

section is just as easily applied to two arbitrary, nonidentical, biaxial ellipsoids, and accordingly we adopt a more general notation.

The approach we adopt is simple. We take one ellipsoid as defining the reference frame for our manipulations, and we scale all three coordinate axes independently to take the reference ellipsoid into a sphere of unit radius. This takes the oriented ellipsoid into a new, biaxial ellipsoid, with dimensions that will depend upon its orientation as well as its original, unscaled dimensions. The problem then becomes one of determining the overlap volume of a sphere and a biaxial ellipsoid, which is equivalent to determining the volume of the parallel body of the biaxial ellipsoid. Standard formulas may be applied, and the resulting overlap volume rescaled to recover the overlap volume of interest. Details follow.

Consider two ellipsoids of semiaxes (a_1,b_1,c_1) and (a_2,b_2,c_2), respectively. We take ellipsoid 1 as defining the space-fixed frame, and we use the Euler angles $\mathbf{\Omega}=\varphi\theta\psi$[33] to define the orientation of ellipsoid 2 with respect to it. Thus ellipsoid 2 defines the surface

$$(\mathbf{r}-\mathbf{r}_2)^T\mathbf{A}_2(\mathbf{r}-\mathbf{r}_2)=1, \tag{8}$$

where $\mathbf{r}_2$ is the coordinate of the center of the ellipsoid. $\mathbf{A}_2$ is the matrix of the quadratic form for the oriented ellipsoid; it may be expressed

$$\mathbf{A}_2=\mathbf{R}\mathbf{D}_2\mathbf{R}^T, \tag{9}$$

where $\mathbf{D}_2$ is the diagonal matrix diag$(a_2^{-2},b_2^{-2},c_2^{-2})$ and $\mathbf{R}$ is the rotation matrix corresponding to the Euler angles $\varphi\theta\psi$. The coordinate scaling that takes ellipsoid 1 into a unit sphere takes ellipsoid 2 into a form characterized by the matrix $\tilde{\mathbf{A}}_2$

$$\tilde{\mathbf{A}}_2=\mathbf{S}\mathbf{A}_2\mathbf{S}, \tag{10}$$

where $\mathbf{S}$ is the scaling matrix diag(a_1,b_1,c_1). The excluded volume of a sphere and the ellipsoid defined by $\tilde{\mathbf{A}}_2$ can be expressed in terms of the fundamental measures of the ellipsoid[34]

$$\tilde{V}_{\rm excl}=\tilde{V}_2+\tilde{S}_2 r+\tilde{M}_2 r^2+\frac{4\pi}{3}r^3, \tag{11}$$

where $r=1$ for the unit sphere. Here $\tilde{V}_2$, $\tilde{S}_2$, and $\tilde{M}_2$ are, respectively, the volume, surface area, and mean radius of curvature of the scaled ellipsoid. These may be evaluated in terms of its semiaxes $(\tilde{a}_2,\tilde{b}_2,\tilde{c}_2)$, defined such that $\tilde{a}_2\leqslant\tilde{b}_2\leqslant\tilde{c}_2$. If $\lambda_a\geqslant\lambda_b\geqslant\lambda_c$ are the eigenvalues of $\tilde{\mathbf{A}}_2$, then

$$(\tilde{a}_2,\tilde{b}_2,\tilde{c}_2)=(\lambda_a^{-1/2},\lambda_b^{-1/2},\lambda_c^{-1/2}). \tag{12}$$

The volume is easy

$$\tilde{V}_2=\frac{4\pi}{3}\tilde{a}_2\tilde{b}_2\tilde{c}_2. \tag{13}$$

The surface area is expressed in terms of elliptic integrals.[35,36] It is useful first to define the eccentricities

$$\epsilon_b=\left(\frac{\tilde{b}_2}{\tilde{a}_2}\right)^2-1, \quad \epsilon_c=\left(\frac{\tilde{c}_2}{\tilde{a}_2}\right)^2-1,$$

then

$$\tilde{S}_2=2\pi\tilde{a}_2\tilde{b}_2\left(\frac{\tilde{a}_2}{\tilde{b}_2}+\epsilon_c^{-1/2}F(\varphi|m)+\epsilon_c^{1/2}E(\varphi|m)\right), \quad (14)$$

where $m=(\tilde{c}_2/\tilde{b}_2)^2\epsilon_b/\epsilon_c$, $\varphi=\tan^{-1}(\epsilon_c^{1/2})$, and F and E are elliptic integrals of the first and second kind, respectively

$$F(\varphi|m)=\int_0^{\varphi}d\theta(1-m\ \sin^2\ \theta)^{-1/2},$$

$$E(\varphi|m)=\int_0^{\varphi}d\theta(1-m\ \sin^2\ \theta)^{1/2}.$$

The mean radius of curvature is given as the integral of the support function over all directions;[34] using Tjipto-Margo and Evans' expression for the support function of a biaxial ellipsoid,[29] $\tilde{M}_2$ is

$$\tilde{M}_2=\tilde{a}_2\int_0^{2\pi}d\varphi\int_0^{\pi}\sin\ \theta\ \ d\theta(1+\epsilon_b\ \sin^2\ \varphi\ \sin^2\theta + \epsilon_c\ \cos^2\theta)^{1/2}. \quad (15)$$

If the integral over θ is taken analytically, $\tilde{M}_2$ may be evaluated by a one-dimensional numerical quadrature

$$\tilde{M}_2=2\tilde{a}_2\int_0^{\pi}d\varphi\left[(P+Q)^{1/2}+\frac{P}{Q^{1/2}}\ln\frac{Q+Q^{1/2}(P+Q)^{1/2}}{(PQ)^{1/2}}\right], \quad (16)$$

where $P(\varphi)=1+\epsilon_b\ \sin^2\varphi$ and $Q(\varphi)=\epsilon_c-\epsilon_b\ \sin^2\varphi$, and we have exploited the symmetry of the integrand to halve the region of integration.

The excluded volume of the two original ellipsoids is recovered by removing the scaling from $\tilde{V}_{\rm excl}$

$$V_{\rm excl}(\mathbf{\Omega})=a_1b_1c_1\tilde{V}_{\rm excl}(\mathbf{\Omega}) \quad (17)$$

and B_2 is obtained directly: $B_2=\frac{1}{2}V_{\rm excl}$. This result (i.e., the uniaxial special case $\mathbf{\Omega}\rightarrow\mathbf{e}\equiv\varphi\theta$, $b_1=c_1$, $b_2=c_2$) may be inserted into Eq. (3) for B_2 given an orientational distribution function $f(\mathbf{e})$. We note that the *isotropically* averaged excluded volume is expressed directly in terms of the fundamental measures of the two ellipsoids, as given by Kihara[34]

$$\overline{B_2^{\rm iso}}=\frac{1}{2}\left(V_1+V_2+\frac{1}{4\pi}(M_1S_2+M_2S_1)\right). \quad (18)$$

This algorithm is easily programmed as a subroutine for use in the numerical calculation of the Onsager/Parsons treatments of the isotropic–nematic transition. It applies generally to all biaxial ellipsoids, and works well even for the most extreme shapes. No doubt certain efficiencies could be introduced in the development, and with some effort the results might be cast in a more explicit form. However, this algorithm proved sufficiently rapid for our purposes. Our numerical calculations are described in the following section.

D. Numerical details

In this study the Onsager and Parsons theories were each carried out for hard ellipsoids of revolution with $5\leqslant x\leqslant 1000$, thus approaching the Onsager limit.

The integral equations for the orientation distribution [Eqs. (4d) and (6d) for the Onsager and Parsons methods, respectively] were solved numerically. The ODF was represented by n points taken uniformly over the (one-dimensional) θ-range of $\mathbf{e}=\theta\varphi$; it is independent of φ. Taking an initial guess $f(\theta,\varphi)=3\ \cos^2\theta/4\pi$, Eq. (4d) or (6d) was solved for the n discretization values by successive substitution. The integrals in these equations were evaluated using Simpson's three-eighths rule, and the orientation-dependent B_2 was computed as described in the previous section. Most calculations were performed taking $n=40$; a few checks made using $n=100$ showed no significant change in the results. Convergence of the ODF was taken when no discretization value changed by more than 10^{-8} over successive iterations.

For comparison, we also used the expansion formulation of trial ODFs with up to 10th-order Legendre polynomials. The initial trial ODF was that in the perfectly aligned limit. The self-consistency equations were iterated until the normalization constant of the ODF had converged to within 10^{-6}.

The coexistence densities were computed as follows. At a trial value of the nematic density, the ODF was calculated, and B_2 for the nematic phase was computed from Eq. (3) with Simpson's-rule integration. The corresponding nematic pressure and chemical potential were computed using the appropriate equations [Eqs. (4b) and (4c), or (6b) and (6c)] with the nematic ODF and B_2. Two isotropic densities corresponding to these values of P and μ were calculated from the same equations, with $f(\mathbf{e})=1/4\pi$ and the isotropically averaged B_2 given by Eq. (18). For coexistence, the two isotropic densities should be equal. The trial nematic density was updated with a bisection method until the difference between the two isotropic densities was less than 10^{-6}.

III. SIMULATION TECHNIQUES

In this section we describe some features of the simulation techniques employed in this study. The Gibbs ensemble simulations were carried out in a standard fashion, and we simply give the relevant details in Sec. IV. To calculate the chemical potential at designated state points, we used either direct test particle insertion, or a version of the force-balance approach due to Attard, and this latter technique is described in Sec. III. Following this, and fitting of the equation of state in the neighborhood of interest, the chemical potential was evaluated using the expression

$$\mu(P)=\mu_0+\int_{P_0}^{P}\frac{dP}{\rho}, \quad (19)$$

where μ_0 is the chemical potential calculated as just men-

tioned at a reference pressure P_0. The coexistence conditions were then solved for $\rho_{\rm iso}$ and $\rho_{\rm nem}$, the isotropic and nematic coexistence densities, respectively,

$$P_{\rm iso}(\rho_{\rm iso}) = P_{\rm nem}(\rho_{\rm nem}), \tag{20}$$

$$\mu_{\rm iso}(\rho_{\rm iso}) = \mu_{\rm nem}(\rho_{\rm nem}). \tag{21}$$

In this way we located the transition point for the chosen elongation, and this constituted the starting point for the Gibbs–Duhem runs. Describing the formulation and implementation of the Gibbs–Duhem technique for these systems is the main objective in Secs. III B–III E.

A. Force-balance method

The force-balance technique was introduced by Attard[5] as a robust way of measuring the chemical potential of fluids. One of the N particles in a conventional MC simulation is designated the ''cavity,'' with a variable size characterized by a scaling parameter κ which takes values $0 \leqslant \kappa \leqslant 1$. At the lower limit, $\kappa = 0$ corresponds to a point particle: the chemical potential of this species is exactly calculable. At the upper limit, $\kappa = 1$ corresponds to a full-sized particle; a set of (typically 10–20) intermediate values of κ is defined at the start of the simulation. During the simulation, standard Monte Carlo moves are supplemented by attempted transitions between κ-states of the cavity particle. A probability histogram $\mathcal{P}(\kappa)$ is constructed of κ-state populations during the simulation. This can be used to calculate the free energy $\mathcal{F}(\kappa)$ for each species, and in particular for $\kappa = 1$, relative to point particles, and hence the chemical potential. To ensure adequate sampling of all the κ values, a weighting function $\mathcal{W}(\kappa)$ is introduced into the acceptance/rejection criterion for κ transitions, and a corresponding correction factor introduced in the calculation of chemical potential. Scaled-particle theory may be used to give a reasonable first estimate of the weighting function; full details are provided by Attard.[5]

We have adopted this scheme, and improved its efficiency in the following ways. First, we progressively refine the weighting function as originally envisaged by Attard,[5] by conducting a series of preliminary simulations and using the ''entropy sampling'' prescription of Lee.[37] In each simulation, conducted with weighting function $\mathcal{W}(\kappa)$, we accumulate an un-normalized probability histogram $\mathcal{P}'(\kappa)$, i.e., the number of occurrences of each κ-state. Then, for the next simulation run, $\mathcal{W}(\kappa)$ is replaced by $\mathcal{W}(\kappa) - k_{\rm B}T \ln \mathcal{P}'(\kappa)$ wherever $\mathcal{P}'(\kappa)$ is nonzero, otherwise it is left unaltered. After a few iterations, the weighting function generates essentially uniform sampling over the range of cavity particle sizes, and ultimately gives a good estimate of the chemical potential.

Second, we attempt to improve the sampling of cavity particle positions, to avoid the danger of the cavity remaining essentially static, and interacting with only a localized region of the simulated fluid. Every MC sweep consists of conventional moves of cavity and normal particles, plus an attempted exchange of the cavity position with a randomly selected full particle, and in addition an attempt to relocate it to a randomly selected position in the box. These moves are unbiased: They are rejected if they incur an overlap, and accepted otherwise. The rationale is that the particle exchanges will be accepted frequently when κ is high, while the random relocations will succeed when κ is low. Between them, these moves ensure that the cavity particle moves rapidly around the entire sample.

B. Gibbs–Duhem integration

Having established the location of the I-N transition for a particular ellipsoid elongation x, we use the Gibbs–Duhem method to move along the coexistence line in the $P-x$ diagram. In other words, we seek a Clapeyron-type differential equation for the coexistence pressure, as a function of ellipsoid elongation.

Consider a one-component system with two coexisting phases, denoted by α and γ, having equal $TP\mu$. An infinitesimal change in any of the thermodynamic variables, maintaining the coexistence conditions, must result in equal changes of the chemical potentials in both phases

$$d\mu_\alpha = d\mu_\gamma . \tag{22}$$

These total derivatives can be written in terms of partial derivatives with respect to the thermodynamic variables. We shall choose P and an as-yet-unspecified variable, λ, which characterizes the particle anisotropy.

$$d\mu = \left(\frac{\partial \mu}{\partial \lambda}\right)_{T,P} d\lambda + \left(\frac{\partial \mu}{\partial P}\right)_{T,\lambda} dP = \Gamma\, d\lambda + v\, dP, \tag{23}$$

where we use the thermodynamic relations $(\partial\mu/\partial P)_{T,\lambda} = 1/\rho = v$, the volume per particle, and $(\partial\mu/\partial\lambda)_{T,P} \equiv \Gamma$, defining a thermodynamic variable Γ conjugate to λ. Equation (22) becomes

$$\Gamma_\alpha\, d\lambda + v_\alpha\, dP = \Gamma_\gamma\, d\lambda + v_\gamma\, dP, \tag{24}$$

from which we obtain a Clapeyron-type equation,

$$\frac{dP}{d\lambda} = -\frac{\Delta\Gamma}{\Delta v}, \tag{25}$$

where

$$\Delta\Gamma = \Gamma_\gamma - \Gamma_\alpha, \tag{26a}$$

$$\Delta v = v_\gamma - v_\alpha = \frac{1}{\rho_\gamma} - \frac{1}{\rho_\alpha}. \tag{26b}$$

Equation (25) represents a first-order differential equation which describes how the pressure of two coexisting phases changes with the thermodynamic variable, λ. As noted in Refs. 8 and 9, if Eq. (25) is written

$$\frac{d \ln P}{d\lambda} = -\frac{\Delta\Gamma}{P\, \Delta v}, \tag{27}$$

the right-hand side (integrand) is a smoother function than that of Eq. (25). All numerical integration techniques benefit from a slowly varying integrand, and so this is the governing differential equation we use here.

C. Calculation of Γ: The general case

To calculate Γ we must relate it to a mechanical quantity measurable in a simulation. First, we note that $G=\mu N$, where G is the Gibbs free energy and N is the number of particles, and so

$$\Gamma=\frac{1}{N}\left(\frac{\partial G}{\partial \lambda}\right)_{T,P}. \tag{28}$$

Next, we express G in terms of the isothermal–isobaric partition function, $\Delta(N,P,T;\lambda)$, for a particular system specified by the anisotropy parameter, λ,

$$G=-k_BT\ \ln\ \Delta(N,P,T;\lambda), \tag{29}$$

with $\Delta(N,P,T;\lambda)$ given by

$$\begin{aligned}\Delta(N,P,T;\lambda)&=\int dV\ \exp\{-\beta PV\}Q(N,V,T;\lambda)\\&=\frac{1}{\Lambda^{3N}N!}\int dV\ \exp\{-\beta PV\}\\&\quad\times\int d\mathbf{r}^N\exp\{-\beta U(\mathbf{r}^N;\lambda)\},\end{aligned} \tag{30}$$

where $\beta=1/k_BT$. In the equations above $Q(N,V,T;\lambda)$ is the canonical partition function for a system with anisotropy parameter λ, Λ is the de Broglie thermal wavelength, $\mathbf{r}^N$ is the set of configuration space coordinates and $U(\mathbf{r}^N)$ is the configurational energy. Note that the prefactor arising from kinetic part of the Hamiltonian is independent of λ. We can now recast Eq. (28) in terms of $\Delta(N,P,T;\lambda)$

$$\begin{aligned}\Gamma&=-\lim_{\delta\lambda\to 0}\frac{k_BT}{N\delta\lambda}\frac{\int dV\ \exp\{-\beta PV\}\int dr^N\ \exp\{-\beta U(\mathbf{r}^N;\lambda+\delta\lambda)\}}{\int dV\ \exp\{-\beta PV\}\int d\mathbf{r}^N\ \exp\{-\beta U(\mathbf{r}^N;\lambda)\}}\\&=-\lim_{\delta\lambda\to 0}\frac{k_BT}{N\delta\lambda}\frac{\int dV\ \exp\{-\beta PV\}\int d\mathbf{r}^N\ \exp\{-\beta[U(r^N;\lambda)+\Delta U]\}}{\int dV\ \exp\{-\beta PV\}\int d\mathbf{r}^N\ \exp\{-\beta U(r^N;\lambda)\}}\\&=-\lim_{\delta\lambda\to 0}\frac{k_BT}{N\delta\lambda}\ln\langle\exp\{-\beta\Delta U\}\rangle,\end{aligned} \tag{31}$$

where ΔU is the change in configurational energy upon changing λ to $\lambda+\delta\lambda$.

D. Calculation of Γ: The hard ellipsoid fluid

We now turn to the calculation of Γ in a fluid of hard uniaxial ellipsoids. Here we use the method pioneered by Eppenga and Frenkel,[38] and Perram and Wertheim,[39,40] to measure the pressure in a constant volume simulation. Throughout our simulations we choose the semiaxes a and b such that $8ab^2=1$. The molecular volume of the ellipsoid, v_0, is therefore equal to that of a hard sphere with unit diameter ($v_0=\pi/6$), and the close-packed density $\rho_{cp}=\sqrt{2}$ irrespective of elongation. The molecular volume is conserved when altering the elongation, and so as a, say, increases b must decrease. We must take into account both of these changes in the calculation of Γ. In practice we chose to alter $\lambda=\ln b$ as the thermodynamic variable, since this simplifies the computation. Γ is calculated in terms of partial derivatives;

$$\begin{aligned}\Gamma&=\left(\frac{\partial\mu}{\partial\ \ln b}\right)_{P,v_0}\\&=\left(\frac{\partial\mu}{\partial\ \ln b}\right)_{P,a}+\left(\frac{\partial\mu}{\partial\ \ln a}\right)_{P,b}\left(\frac{d\ \ln a}{d\ \ln b}\right)=\Gamma_b-2\Gamma_a,\end{aligned} \tag{32}$$

where

$$\Gamma_a=\left(\frac{\partial\mu}{\partial\ \ln a}\right)_{P,b}\qquad\Gamma_b=\left(\frac{\partial\mu}{\partial\ \ln b}\right)_{P,a}. \tag{33}$$

To calculate Γ_b (and similarly Γ_a), we note that for hard particle systems, Eq. (31) is equivalent to

$$\Gamma_b=-\lim_{\delta\lambda\to 0}\frac{k_BT}{N\delta\lambda}\ln\mathcal{P}_b^{\text{accept}},\quad \lambda\equiv\ln b,\ \text{with}\ a\ \text{fixed}. \tag{34}$$

$\mathcal{P}_b^{\text{accept}}$ is the probability of accepting the ghost change $\ln b\to\ln b+\delta\lambda$, holding a fixed, without overlap between any pair of particles. $\mathcal{P}_b^{\text{accept}}$ can be expanded in terms of the probability of overlap between a pair of particles, i and j, denoted by $\mathcal{P}_{b,ij}^{\text{overlap}}$:

$$\mathcal{P}_b^{\text{accept}}=\prod_{i>j}(1-\mathcal{P}_{b,ij}^{\text{overlap}})\approx 1-\sum_{i>j}\mathcal{P}_{b,ij}^{\text{overlap}}. \tag{35}$$

We now identify $\mathcal{P}_{b,ij}^{\text{overlap}}$ with the ensemble average of the number of overlaps upon the particle scaling $\ln b\to\ln b+\delta\lambda$

$$\mathcal{P}_{b,ij}^{\text{overlap}}=\frac{\langle N_b^{\text{overlap}}\rangle}{\frac{1}{2}N(N-1)}. \tag{36}$$

Equation (35) can now be expressed in terms of an ensemble average

$$\mathcal{P}_b^{\text{accept}} = 1 - \sum_{i>j} \frac{\langle N_b^{\text{overlap}} \rangle}{\frac{1}{2}N(N-1)} = 1 - \langle N_b^{\text{overlap}} \rangle. \tag{37}$$

Using the fact that $\delta\lambda$ should be small, we can substitute Eq. (37) into Eq. (34) and expanding the logarithm to lowest order gives,

$$\Gamma_b = \lim_{\delta\lambda \to 0} k_B T \frac{\langle N_b^{\text{overlap}} \rangle}{N \delta\lambda}. \tag{38}$$

The calculation of Γ_b in a simulation is thus carried out as follows. The minor semiaxis, b, is scaled by a factor of $(1+\delta\lambda)$, where $\delta\lambda$ is small and positive, with a held constant. The number of pair overlaps, N_b^{overlap} is then determined; b is then returned to its appropriate value for the current ellipsoid anisotropy. a is scaled in a similar fashion and the number of pair overlaps, N_a^{overlap}, counted. The instantaneous value of Γ is then calculated and accumulated as a simulation average,

$$\Gamma = \frac{k_B T}{N \delta\lambda} \langle N_b^{\text{overlap}} - 2N_a^{\text{overlap}} \rangle, \tag{39}$$

which is equivalent to Eq. (32).

E. The integrator

Starting from a simulation of both phases at the known coexistence pressure P for a given elongation parameter λ, we wish to move to a new transition pressure P' corresponding to new elongation $\lambda + \Delta\lambda$, where $\Delta\lambda$ is the chosen step size in $\lambda = \ln b$. Having evaluated Γ, and the volume per particle $v = 1/\rho$, in both simulation boxes at pressure P, we evaluate the right-hand side (rhs) of Eq. (27), which we denote Φ. There are many numerical techniques available for solving first-order differential equations. In this work we employ a straightforward trapezoid predictor–corrector method. The new coexistence pressure, P' is predicted by

$$P' = P \exp\{\Phi \Delta\lambda\}. \tag{40}$$

Next, a corrector stage is performed where the running average of the rhs of Eq. (27), denoted by Φ', is used to correct the predicted pressure

$$P' = P \exp\{\tfrac{1}{2}\Delta\lambda(\Phi + \Phi')\}. \tag{41}$$

To do this, a simulation is started at a pressure P' and a running average of Φ' is accumulated over a number of MC sweeps, after which the pressure is corrected as in Eq. (41). This process is repeated until successive corrected pressures converge within a given tolerance. Note that the values P and Φ do not change during the course of a simulation: They are the values for the previous elongation. A production run at this corrected pressure provides a new integrand by which the next coexistence pressure is predicted.

IV. SIMULATION RUNS

We describe here the calculations of chemical potentials and the Gibbs ensemble simulations, used to provide starting points for the Gibbs–Duhem integrations. Then we give full details of the Gibbs–Duhem integrations themselves. Except as outlined above, standard hard-particle Monte Carlo and molecular dynamics simulation techniques were used.[17,41] Throughout this work, truncated octahedral periodic boundary conditions were employed, and we used both the equivalent ellipsoid overlap criteria due to Perram and Wertheim[39,40] and Vieillard-Baron.[42,43]

TABLE II. Chemical potentials for various hard ellipsoid fluids. The abbreviations are as follows: FB (force-balance Monte Carlo), TI (thermodynamic integration), PI (particle insertion), GS (Gibbs simulation).

x	ρ/ρ_{cp}	μ	Method
5	0.450	11.35	FB
5	0.550	15.33	FB
5	0.505	14.40	TI
5	0.531	14.40	TI
20	0.100	2.61	PI
20	0.213	6.60	PI
20	0.153	6.06	TI
20	0.184	6.06	TI
20	0.153	6.04	GS
20	0.183	6.04	GS

A. Starting points

We have determined the chemical potential in the isotropic and nematic phases using the force-balance method of Attard[5] (see Sec. III A) for $x=5$, and by direct test particle insertion for $x=20$. In each case, equation-of-state data in both phases were used to locate the coexistence points by thermodynamic integration. The transition at $x=20$ was also located directly by Gibbs ensemble simulation.

The chemical potential for $x=5$ was determined at $\rho/\rho_{cp}=0.45$ (isotropic phase) and $\rho/\rho_{cp}=0.55$ (nematic phase). We used constant-NVT MC with $N=216$ particles; the ''cavity'' particle was allowed 14 values of scaling parameter κ between a point particle ($\kappa=0$) and full size ($\kappa=1$). Translational and rotational displacements were chosen so as to give an acceptance ratio in the range 40%–50%. The biasing function for κ moves was estimated initially by an equilibration run of 125 000 MC sweeps, and was refined throughout five production runs each consisting of 250 000 MC sweeps. The results for the chemical potential are shown in Table II.

Accurate equation-of-state data for the $x=5$ system have been reported previously[18,44] but extra data close to the I-N transition were needed. We have carried out molecular dynamics (MD) simulations at $x=5$ at many state points in and around the I-N coexistence region, $0.45 \leqslant \rho/\rho_{cp} \leqslant 0.55$. We used a system size $N=216$, and run lengths in the range $1-3 \times 10^5$ collisions per particle; close to the transition it was essential to allow such long times for the system to equilibrate. The results are shown in Table III and Fig. 1. Also shown in the table is the nematic order parameter, S, defined in Eq. (5), and calculated from the highest eigenvalue of the second-rank order tensor.[38,45] For macroscopic systems, the isotropic phase is characterised by $S=0$, and the perfectly

TABLE III. Equation of state data for the $x=5$ hard ellipsoid fluid from MD and MC simulation ($N=216$). We give the density ρ as a fraction of close-packed density, pressure P and nematic order parameter S. Results marked with an asterisk (*) are from MC simulation (Refs. 18 and 44). Estimated errors in the last digit are in parentheses.

ρ/ρ_{cp}	P	S	ρ/ρ_{cp}	P	S
*0.450	5.34(2)	0.13(1)	0.510	7.08(2)	0.505(8)
*0.475	6.22(3)	0.16(1)	0.511	7.10(2)	0.517(8)
0.480	6.427(6)	0.175(4)	0.512	7.08(2)	0.541(6)
0.484	6.559(8)	0.195(7)	0.513	7.11(2)	0.545(8)
0.488	6.69(1)	0.221(7)	0.514	7.10(2)	0.565(7)
0.492	6.85(1)	0.221(9)	0.515	7.18(2)	0.549(7)
0.496	6.90(2)	0.30(1)	0.516	7.13(1)	0.581(5)
0.500	7.02(1)	0.330(9)	0.518	7.17(1)	0.598(4)
0.502	7.03(2)	0.37(1)	0.520	7.22(1)	0.609(4)
0.503	7.01(2)	0.40(1)	0.522	7.23(1)	0.632(3)
0.504	7.05(2)	0.40(1)	*0.525	7.36(9)	0.63(3)
0.505	7.06(2)	0.42(1)	0.530	7.44(3)	0.67(1)
0.506	7.05(2)	0.44(1)	0.535	7.58(2)	0.688(7)
0.507	7.06(2)	0.46(1)	0.540	7.74(3)	0.706(7)
0.508	7.08(2)	0.470(9)	0.545	7.88(4)	0.73(1)
0.509	7.06(2)	0.499(7)	*0.550	8.14(7)	0.70(4)

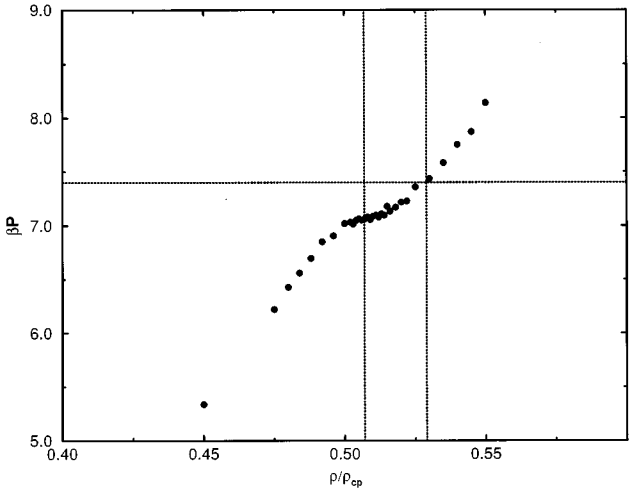

FIG. 1. Equation of state data for the $x=5$ hard ellipsoid fluid from MD simulation ($N=216$) (points). Coexistence data from thermodynamic integration are indicated by the dotted lines.

aligned nematic phase by $S=1$. Finite-size effects are apparent in the order parameters, however, in the sense that even in the isotropic phase they take values $\mathcal{O}(N^{-1/2})$.

After fitting the equation of state, the values of T and P satisfying the thermodynamic coexistence conditions were calculated. I-N coexistence data for the $x=5$ hard ellipsoid fluid are presented in Tables II and VI.

Equation-of-state data for the $x=20$ system were obtained by constant-volume and constant-pressure MC simulations of $N=500$ particles and are presented in Table IV and Fig. 2. We used approximately 50 000 MC sweeps at each state point. The chemical potential was determined using Widom test particle insertion[3] using 500 attempts per MC sweep. The results are shown in Table II.

At this point we note that the system sizes were chosen to avoid interactions between periodic images. Such interactions are avoided if $2a<r_{ins}$, where r_{ins} is the radius of the inscribed sphere in the truncated octahedral simulation cell. This is given by

$$r_{ins}=\sqrt{3}L/4, \tag{42}$$

where L is the length of the cube containing the truncated octahedral simulation cell. As can be seen from Table V, the system size for the $x=20$ simulations was too small to avoid periodic image interactions for the most unfavourable orientations of particles. However, the results are in good agreement with Gibbs simulations carried out with a larger system, which we shall now describe, and we believe that the system size effects are small.

In the $x=20$ system, the I-N transition occurs at sufficiently low density for the Gibbs ensemble method[6,7] to be practicable. The simulation was started with $N=1000$ particles in each box, and the box size was large enough to completely rule out interactions between periodic images

TABLE VI. Coexistence data for the isotropic–nematic phase transition in hard ellipsoids at various elongations. All results are obtained by Gibbs–Duhem integration except for † (thermodynamic integration) and ‡ (Gibbs simulation). Estimated errors in the last digit are in parentheses.

x	N	P	Γ_{iso}	ρ_{iso}/ρ_{cp}	μ_{iso}	Γ_{nem}	ρ_{nem}/ρ_{cp}	μ_{nem}	S
5.000†	216	7.40	−10.5(4)	0.507(5)	14.40	−8.3(6)	0.529(6)	14.40	0.66
5.743	216	5.84	−10.7(5)	0.454(4)	12.57	−8.1(5)	0.482(9)	12.59	0.66
6.597	216	4.59	−10.8(3)	0.400(3)	10.98	−8.1(6)	0.433(6)	11.02	0.65
7.579	500	3.70	−10.2(5)	0.361(5)	9.81	−7.5(4)	0.391(4)	9.86	0.69
8.706	500	3.03	−10.1(5)	0.321(5)	8.87	−7.7(4)	0.350(5)	8.93	0.71
10.00	500	2.50	−9.9(3)	0.283(3)	8.09	−7.2(2)	0.321(4)	8.17	0.69
10.00	1000	2.48	−10.0(3)	0.284(2)	8.38	−7.2(3)	0.321(3)	8.33	0.75
11.49	1000	1.93	−9.6(2)	0.242(1)	7.34	−7.9(4)	0.274(2)	7.35	0.69
13.20	1000	1.71	−9.9(3)	0.219(1)	7.10	−7.1(2)	0.256(4)	7.09	0.74
15.16	1000	1.47	−9.8(2)	0.194(1)	6.75	−7.1(2)	0.230(1)	6.74	0.75
17.41	1000	1.28	−9.4(3)	0.167(2)	6.44	−7.1(2)	0.194(2)	6.42	0.73
20.00†	500	1.10	−9.6(1)	0.153(1)	6.06	−7.2(1)	0.184(1)	6.06	
20.00‡	1000			0.153(1)	6.04(4)		0.183(1)	6.04(4)	0.75

TABLE IV. Equation of state data for the $x=20$ hard ellipsoid fluid from MC simulation ($N=500$). We give the density ρ as a fraction of close-packed density, pressure P and nematic order parameter S. V denotes constant-volume MC simulations, P denotes constant-pressure MC simulations.

ρ/ρ_{cp}	P	S	Ens.	ρ/ρ_{cp}	P	S	Ens.
0.1000	0.482	0.040	V	0.1700	1.085	0.665	V
0.1100	0.577	0.048	V	0.1800	1.113	0.740	V
0.1200	0.684	0.049	V	0.1830	1.113	0.766	P
0.1291	0.805	0.039	P	0.1850	1.150	—	P
0.1300	0.806	0.039	V	0.1900	1.146	0.803	V
0.1395	0.920	0.064	P	0.1940	1.146	0.796	P
0.1400	0.919	0.055	V	0.2000	1.234	0.825	V
0.1498	1.059	0.105	P	0.2110	1.237	0.860	P
0.1500	1.058	0.098	V	0.2130	1.275	0.863	P
0.1530	1.150	—	P	0.2400	1.400	0.902	P
0.1600	1.187	0.227	V	0.2500	1.500	0.913	P

(see Table V). We carried out an equilibration run of 5000 MC sweeps and a production run of another 5000 MC sweeps over which the coexistence densities were averaged. Each MC sweep consisted of an attempt to translate and rotate each particle in each box (displacement parameters chosen to give a 40%–50% acceptance ratio), a conservative volume exchange between the boxes, and 50 000 attempts to transfer particles in a random direction between the boxes. With this number of transfer attempts, 1%–2% of the total number of particles were transferred, on average, per MC sweep. In Fig. 2, density histograms from Gibbs simulation are superimposed on the equation of state, showing good agreement with the coexistence data from thermodynamic integration. The chemical potential was calculated within the Gibbs ensemble using the expression given by Smit and Frenkel.[46] The results are shown in Table II. I-N coexistence data for the $x=20$ hard ellipsoid fluid are presented in Table VI.

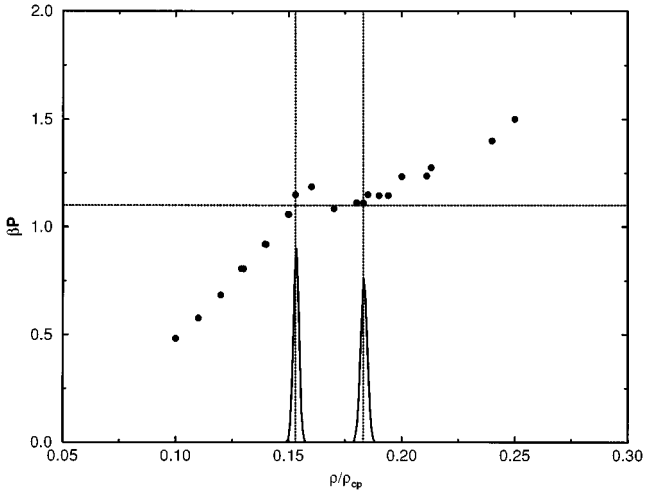

FIG. 2. Equation of state data for the $x=20$ hard ellipsoid fluid from constant-volume and constant-pressure MC simulations ($N=500$) (points), with the density histogram from Gibbs simulation (solid line). Coexistence data from thermodynamic integration are indicated by the dotted lines.

B. Gibbs–Duhem runs

Gibbs–Duhem simulations were conducted, integrating along the isotropic–nematic coexistence line from $x=5$ to $x=10$ and from $x=20$ to $x=10$, using starting values determined as described above.

Constant-pressure MC simulations were performed in each phase simultaneously with system sizes between $N=216$ and $N=1000$, depending on elongation (see below). Each MC sweep consisted of an attempted translation and rotation per particle (displacement parameters chosen to give a 40%–50% acceptance ratio), and an attempted volume change. To calculate Γ, every 10 MC sweeps the ellipsoid dimensions were scaled and the number of resulting overlaps counted, as outlined in Sec. III C, with $\delta\lambda=0.005$. This choice is small enough to give the asymptotic behavior in Eq. (38) but large enough to result in a statistically significant number of overlaps. In the predictor–corrector stage Γ was accumulated as a running average, and the pressure was

TABLE V. Ratios of the ellipsoid length $2a$ and the radius of the inscribed sphere r_{ins} [see Eq. (42)], in the truncated octahedral simulation cell at nematic coexistence densities for systems with elongations in the range $x=5$ to $x=20$. The coexistence data were determined by Gibbs–Duhem integration in all cases (see Table VI) except for † (thermodynamic integration) and ‡ (Gibbs simulation).

N	x	$2a$	ρ_{nem}/ρ_{cp}	$2a/r_{ins}$
216†	5.000	2.924	0.529	0.811
216	5.743	3.207	0.482	0.862
216	6.597	3.517	0.433	0.912
216	7.579	3.858	0.395	0.971
500	7.579	3.858	0.391	0.731
500	8.706	4.232	0.350	0.773
500	10.00	4.642	0.320	0.823
1000	10.00	4.642	0.321	0.653
1000	11.49	5.091	0.274	0.680
1000	13.20	5.584	0.256	0.730
1000	15.16	6.125	0.230	0.772
1000	17.41	6.718	0.194	0.801
500†	20.00	7.368	0.184	1.086
1000‡	20.00	7.368	0.183	0.861

corrected every 10000 MC sweeps until it had converged to within 10^{-3}. The production run, where Γ was accumulated as a block average, consisted of 50 000–80 000 MC sweeps. The integration step size, $\Delta\lambda$, was chosen to be $\frac{1}{15}\ln 2$, which results in five integration steps between $x=5$ and $x=10$, and five more between $x=20$ and $x=10$.

The ratios of the ellipsoid length and $r_{\rm ins}$ [see Eq. (42)] in the nematic phase for $5\leqslant x\leqslant 20$ are shown in Table V. The densities shown in Table V are those at coexistence with the isotropic phase. For the integration from $x=5$ to $x=7.579$ a system size of $N=216$ was sufficient; from this point to $x=10$ a system size $N=500$ was required; between $x=10$ and $x=20$ a system size of $N=1000$ in each phase was needed. System size effects on the chemical potential and pressure may be important in evaluating phase coexistence. Smit and Frenkel have given an explicit expression for the finite-size corrections to the excess chemical potential[47]

$$\Delta\mu_N^{\rm ex}=\frac{[1-k_{\rm B}T\rho\kappa_T]^2}{2N\rho\kappa_T}, \tag{43}$$

where κ_T is the isothermal compressibility

$$\kappa_T=-\frac{1}{V}\left(\frac{\partial V}{\partial P}\right)_T=\frac{\langle\delta V^2\rangle}{Vk_{\rm B}T}, \tag{44}$$

where the last formula applies in the constant-NPT ensemble. To gauge the effect of changing system sizes at $x=7.579$, $\Delta\mu$ was calculated at the relevant coexistence pressure

$$\Delta\mu=\ln(\rho_{216}/\rho_{500})+\Delta\mu_{216}^{\rm ex}-\Delta\mu_{500}^{\rm ex}, \tag{45}$$

where the subscripts denote N. In both the isotropic and nematic phases $\Delta\mu\sim 0.01$, and so the finite-size corrections were deemed to be small compared to the numerical accuracy of the integration technique. We note that a more accurate expression for the finite-size correction to the chemical potential has been given by Siepmann *et al.*,[48] but Smit and Frenkel's result is sufficient to show that it is small in the present case.

V. RESULTS

In Table VI we summarize the coexistence pressure, densities and nematic order parameters at the transition, for $5\leqslant x\leqslant 20$, as determined by Gibbs–Duhem integration. The chemical potentials of the two phases provide a measure of integration accuracy along the coexistence line, and have been calculated simply by integrating Eq. (23) using the trapezoid rule

$$\begin{aligned}\mu_2&=\mu_1+\int_{\lambda_1}^{\lambda_2}\Gamma\,{\rm d}\lambda+\int_{P_1}^{P_2}v\,{\rm d}P\\&\simeq\mu_1+\tfrac{1}{2}(\Gamma_2+\Gamma_1)(\lambda_2-\lambda_1)+\tfrac{1}{2}(v_2+v_1)(P_2-P_1).\end{aligned} \tag{46}$$

At each elongation along both paths $x=5\rightarrow 10$ and $x=20\rightarrow 10$ the chemical potentials in the two phases are equal to within 0.08. The chemical potentials at $x=10$ agree to within 0.29 (isotropic) and to within 0.16 (nematic), which gives an idea of the accumulated errors in this quantity; the coexistence densities are almost identical via both routes.

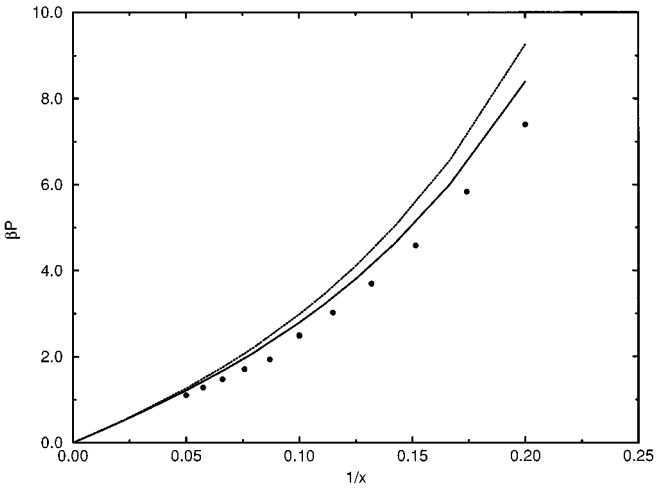

FIG. 3. The isotropic-nematic coexistence pressure versus $1/x$: Gibbs–Duhem integration (points), Parsons theory (solid line), Onsager theory (dotted line).

In Table I we present the corresponding coexistence data predictions from Parsons and Onsager theory, using the ''exact'' expression for $B_2(\mathbf{e}\cdot\mathbf{e}')$ as well as the Legendre expansion, Eq. (7). Clearly the results using the expansion for $B_2(\mathbf{e}\cdot\mathbf{e}')$ are subject to truncation errors as x becomes large, as evidenced by the tabulated values of $B_2^{\parallel}/4v_0$, and so elongations only up to $x=20$ were studied with it. At low x the coexistence results are very similar. From now on we shall only consider those results obtained with the exact values of B_2.

In Fig. 3 the coexistence pressure is shown as a function of $1/x$. The Parsons predictions are seen to represent the simulation results more accurately than the Onsager theory. As x becomes large, the Parsons and Onsager theories converge, signalling the approach to the Onsager limit.

This approach is seen more clearly on a plot of the coexistence densities against $1/x$, as shown in Fig. 4. It is convenient to scale the densities for each elongation by $B_2^{\rm iso}$ as given by Eq. (18). As $1/x\rightarrow 0$, the Parsons results are seen to collapse onto the Onsager predictions in both phases. Specifically, in the Onsager limit, $\rho_{\rm iso}B_2^{\rm iso}=3.291$ and $\rho_{\rm nem}B_2^{\rm iso}=4.209$; the approach of $\rho B_2^{\rm iso}$ in the two phases is shown in Fig. 5. Simulation results are also shown in this figure. In earlier work Lee[26] estimated that the Parsons results, in the case of the hard Gaussian overlap model, collapse onto the Onsager results for $x\geqslant 25$, from a graph similar to Fig. 4. A graph such as Fig. 5 shows this effect much more clearly. The Parsons results are clearly more accurate, with respect to simulation data, than the Onsager predictions away from the Onsager limit, i.e., $5\leqslant x\leqslant 20$.

The nematic order parameter, S, at coexistence is shown as a function of $1/x$ in Fig. 6. The simulation results give an indication of a rise in S as $x\rightarrow\infty$, but statistical errors and finite-size errors preclude a more accurate interpretation. Interestingly the Parsons transition order parameters are higher

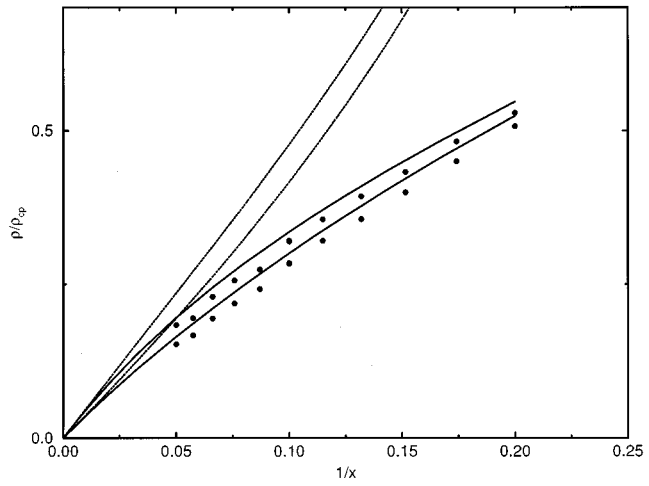

FIG. 4. The isotropic-nematic coexistence densities versus $1/x$: Gibbs–Duhem integration (points), Parsons theory (solid line), Onsager theory (dotted line).

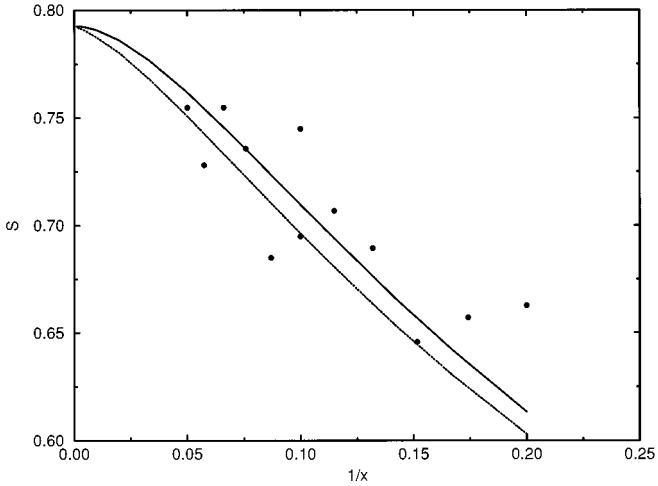

FIG. 6. The nematic order parameters at coexistence versus $1/x$: Gibbs–Duhem integration (points), Parsons theory (solid line), Onsager theory (dotted line).

than the Onsager results at a given elongation, despite the Onsager theory predicting higher nematic coexistence densities. This is due solely to the nature of the transformation between the density variables (those multiplied by B_2) in the Onsager (4a) and Parsons (6a) expressions. The relative density change, $\Delta\rho/\overline{\rho}$, where $\overline{\rho}=(\rho_{\mathrm{iso}}+\rho_{\mathrm{nem}})/2$, predicted by the Parsons theory should be smaller than that predicted by Onsager theory. This is indeed the case, as illustrated in Fig. 7: Onsager theory *overestimates* the strength of the transition, as measured in this way. In terms of the simulation results, the relative density change is a more accurate indicator of the strength of the transition, than the value of the order parameter. The order parameters, S, often used by experimentalists as such an indicator, are significantly higher for these systems than those measured in real mesophases ($S\sim 0.4$).

VI. CONCLUSIONS

We have tested the versatility of the Gibbs–Duhem technique by application to the liquid crystal phase transition in hard uniaxial ellipsoid fluids. The coexistence pressure line as a function of elongation has been mapped out in the range $5\leqslant x\leqslant 20$. Matching the results at $x=10$ from two independent routes has provided a good check on the accuracy of the method. Reference 13 provides an analysis of the error in the initial coexistence pressure carried through the integration, assuming no integration errors. This showed that subsequent estimates of the coexistence pressures will be worse on approach to a weak transition or critical point. On this basis the results from the integration path from $x=5\rightarrow 10$ should, in principle, be slightly more accurate than those from $x=20\rightarrow 10$.

We see the transition weakening with decreasing elongation: The fractional density difference $\Delta\rho/\overline{\rho}$ falls from

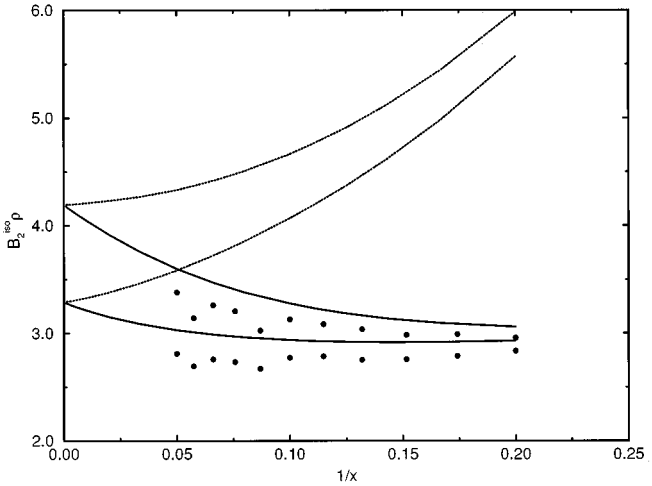

FIG. 5. The isotropic–nematic coexistence densities scaled by $\overline{B_2^{\mathrm{iso}}}$ in the isotropic phase, versus $1/x$: Gibbs–Duhem integration (points), Parsons theory (solid line), Onsager theory (dotted line).

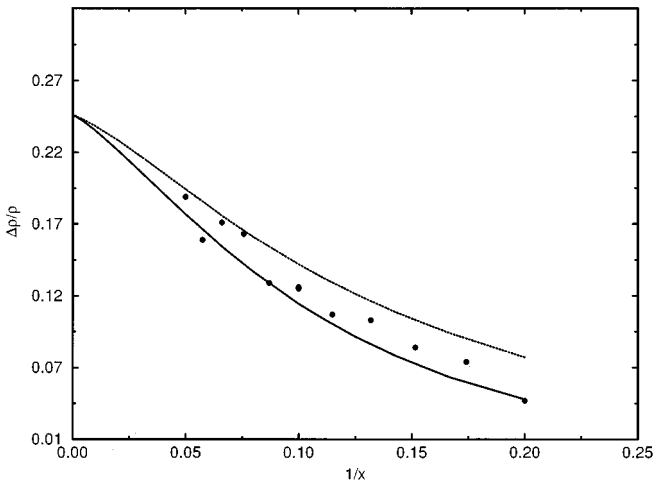

FIG. 7. The percentage density change versus $1/x$: Gibbs–Duhem integration (points), Parsons theory (solid line), Onsager theory (dotted line).

about 18% for $x=20$ through 12% at $x=10$, to about 4% at $x=5$. The transition order parameter S also falls from 0.75 at $x=20$ to 0.66 at $x=5$, but this is not such a dramatic change, and the values are still high compared with those seen in thermotropic liquid crystals.

Simple scaling of the free energy functional for hard ellipsoids, following the prescription of Parsons and Lee, in conjunction with accurate calculations of $\bar{B}_2$, gives results quantitatively comparable with those from computer simulation. The approach to the Onsager limit has, up until now, been blighted by the slow convergence of the expression for the pair excluded volume: The higher order coefficients are more difficult to compute accurately. We have presented an essentially exact expression for the pair excluded volume of two hard ellipsoids which has enabled us to investigate the approach to the Onsager limit with elongations up to $x=1000$.

Several future projects are suggested. The effect of particle biaxiality on the I-N transition in hard ellipsoids could be investigated by integrating from the uniaxial limit: very little work on this particular system has appeared since the first preliminary study.[49] The effect of elongation on the formation of liquid crystalline phases could be investigated in hard ellipsoids, by very careful integration from $x=5$ to lower elongations. The effect on the phase diagram of varying parameters in more realistic intermolecular potentials, for example the Gay–Berne model,[50] following the approach of Refs. 10,11,13, is a further application. Given the large parameter space for systems of this kind, Gibbs–Duhem integration should be an efficient way of mapping out large parts of the phase diagram.

ACKNOWLEDGMENTS

This work was supported by the Engineering and Physical Sciences Research Council through the provision of computer hardware and studentships to C.P.M. and P.J.C. Acknowledgment is made to the Donors of the Petroleum Research Fund, administered by the American Chemical Society, for support of A.A.K. D.A.K. is grateful to the U.S. National Science Foundation for provision of computer hardware. The collaboration was supported by a NATO Travel Grant. We acknowledge helpful conversations with G. T. Evans, D. Frenkel, A. J. Masters, and B. Mulder.

[1] D. Frenkel, Numerical techniques to study complex liquids, in *Observation, Prediction and Simulation of Phase Transitions in Complex Fluids*, edited by M. Baus, L. F. Rull, and J.-P. Ryckaert, Vol. 460, NATO ASI Series C (Kluwer Academic, Dordrecht, 1995), pp. 357–419. Proceedings of the NATO Advanced Study Institute on ''Observation, prediction and simulation of phase transitions in complex fluids,'' Varenna, Italy, July 25–August 5, 1994.

[2] M. P. Allen, Simulation and phase diagrams, in *Monte Carlo and Molecular Dynamics of Condensed Matter Systems*, edited by K. Binder and G. Ciccotti, Proceedings of the Euroconference on ''Monte Carlo and molecular dynamics of condensed matter systems,'' Como, Italy, July 3–28, 1995 (Italian Physical Society, Bologna, 1996), Chap. 10, pp. 255–284.

[3] B. Widom, J. Chem. Phys. **39**, 3197 (1963).

[4] K. K. Mon and R. B. Griffiths, Phys. Rev. A **31**, 956 (1985).

[5] P. Attard, J. Chem. Phys. **98**, 2225 (1993).

[6] A. Z. Panagiotopoulos, Mol. Phys. **61**, 813 (1987).

[7] A. Z. Panagiotopoulos, N. Quirke, M. Stapleton, and D. J. Tildesley, Mol. Phys. **63**, 527 (1988).

[8] D. A. Kofke, Mol. Phys. **78**, 1331 (1993).

[9] D. A. Kofke, J. Chem. Phys. **98**, 4149 (1993).

[10] R. Agrawal, M. Mehta, and D. A. Kofke, Int. J. Thermophys. **15**, 1073 (1994).

[11] R. Agrawal and D. A. Kofke, Mol. Phys. **85**, 23 (1995).

[12] R. Agrawal and D. A. Kofke, Phys. Rev. Lett. **74**, 122 (1995).

[13] R. Agrawal and D. A. Kofke, Mol. Phys. **85**, 43 (1995).

[14] M. Dijkstra and D. Frenkel, Phys. Rev. E **51**, 5891 (1995).

[15] D. Frenkel and B. M. Mulder, Mol. Phys. **55**, 1171 (1985).

[16] M. P. Allen and M. R. Wilson, J. Comput. Aided Mol. Design **3**, 335 (1989).

[17] M. P. Allen, G. T. Evans, D. Frenkel, and B. Mulder, Adv. Chem. Phys. **86**, 1 (1993).

[18] A. Samborski, G. T. Evans, C. P. Mason, and M. P. Allen, Mol. Phys. **81**, 263 (1994).

[19] L. Onsager, Ann. N. Y. Acad. Sci. **51**, 627 (1949).

[20] B. M. Mulder and D. Frenkel, Mol. Phys. **55**, 1193 (1985).

[21] B. Tjipto-Margo and G. T. Evans, J. Chem. Phys. **93**, 4254 (1990).

[22] B. Barboy and W. M. Gelbart, J. Chem. Phys. **71**, 3053 (1979).

[23] B. Barboy and W. M. Gelbart, J. Stat. Phys. **22**, 685 (1980).

[24] B. Barboy and W. M. Gelbart, J. Stat. Phys. **22**, 709 (1980).

[25] J. D. Parsons, Phys. Rev. A **19**, 1225 (1979).

[26] S.-D. Lee, J. Chem. Phys. **87**, 4972 (1987).

[27] S.-D. Lee, J. Chem. Phys. **89**, 7036 (1989).

[28] J.-P. Hansen and I. R. McDonald, *Theory of Simple Liquids*, 2nd ed. (Academic, London, 1986).

[29] B. Tjipto-Margo and G. T. Evans, J. Chem. Phys. **94**, 4546 (1991).

[30] A. Isihara, J. Chem. Phys. **19**, 1142 (1951).

[31] B. M. Mulder, Liq. Cryst. **1**, 539 (1986).

[32] M. P. Taylor, Liq. Cryst. **9**, 141 (1991).

[33] H. Goldstein, *Classical Mechanics*, 2nd ed. (Addison Wesley, Reading, 1980).

[34] T. Kihara, Adv. Chem. Phys. **5**, 147 (1963).

[35] F. Bowman, *Introduction to Elliptic Functions* (Dover, New York, 1961).

[36] G. Dassios, Int. J. Eng. Sci. **28**, 1205 (1990).

[37] J. Lee, Phys. Rev. Lett. **71**, 211 (1993).

[38] R. Eppenga and D. Frenkel, Mol. Phys. **52**, 1303 (1984).

[39] J. W. Perram, M. S. Wertheim, J. L. Lebowitz, and G. O. Williams, Chem. Phys. Lett. **105**, 277 (1984).

[40] J. W. Perram and M. S. Wertheim, J. Comput. Phys. **58**, 409 (1985).

[41] M. P. Allen, Molecular dynamics for hard particles, in *Monte Carlo and Molecular Dynamics of Condensed Matter Systems*, edited by K. Binder and G. Ciccotti, Proceedings of the Euroconference on ''Monte Carlo and molecular dynamics of condensed matter systems,'' Como, Italy, July 3–28, 1995 (Italian Physical Society, Bologna, 1996), Chap. 3, pp. 89–105.

[42] J. Vieillard-Baron, J. Chem. Phys. **56**, 4729 (1972).

[43] J. Vieillard-Baron, Mol. Phys. **28**, 809 (1974).

[44] C. P. Mason, Ph.D. thesis, University of Bristol, 1994.

[45] C. Zannoni, in *The Molecular Physics of Liquid Crystals*, edited by G. R. Luckhurst and G. W. Gray (Academic, New York, 1979), Chap. 3, pp. 191–120.

[46] B. Smit and D. Frenkel, Mol. Phys. **68**, 951 (1989).

[47] B. Smit and D. Frenkel, J. Phys. Cond. Mat. **1**, 8659 (1989).

[48] J. I. Siepmann, I. R. McDonald, and D. Frenkel, J. Phys. Cond. Mat. **4**, 679 (1992).

[49] M. P. Allen, Liq. Cryst. **8**, 499 (1990).

[50] J. G. Gay and B. J. Berne, J. Chem. Phys. **74**, 3316 (1981).